View metadata, citation and similar papers at core.ac.uk
brought to you by CORE
provided by AMS Acta

An overview of low noise devices and associated circuits for 100-200 GHz space applications

Gilles Dambrine[1], Thierry Parenty[1], Sylvain Bollaert[1], Henri Happy[1], A. Cappy[1], Javier Mateos[2], Tapani Nahri[3], Jean Claude Orlhac[4], Marc Trier[4], Pierre Baudet[5], Patrice Landry[6].

[1]I.E.M.N., Avenue Poincaré, BP 69, F-59652, Villeneuve d'Ascq, France, 33 3 20 19 78 61.
[2] Departamento de Física Aplicada Universidad de Salamanca Salamanca, Spain
[3] ESTEC P.O. Box 299, 2200 AG Noordwijk, The Netherlands.
[4] ASTRIUM, 31 Avenue des Cosmonautes, F-31402 Toulouse Cedex 4, France 33 5 62 19 75 70.
[5] OMMIC, . 22 av Descartes BP 11, F-94453 Limeil Brevanne, France.
[6] Observatoire de Paris - Site de Meudon 5, place Jules Janssen, 92195 Meudon.

***Abstract* — This paper relates the state of the art of the HEMT low noise technologies for the space applications at millimeter wave and specially for the earth observation in the G-band (140 – 220 GHz). The different III-V technologies (HEMT and LNA) and their associated performance are presented. Parameters limiting the improvement of high frequency characteristics for HEMTs with the downscaling process are studied.**

I. INTRODUCTION

MM-wave radiometer space applications like atmospheric sounding needs ultra low noise receivers in order to achieve an excellent radiometric sensitivity (brightness temperature resolution). One of these space applications is the Eumetsat [1] Microwave Humidity Sounder (MHS) (see Fig. 1 photograph of the MHS Receiver built by ASTRIUM France). This instrument looks down into the atmosphere and scans the emitted radiation in various spectral bands (mainly in G-band) to determine the water vapor content or humidity profile of the atmosphere.

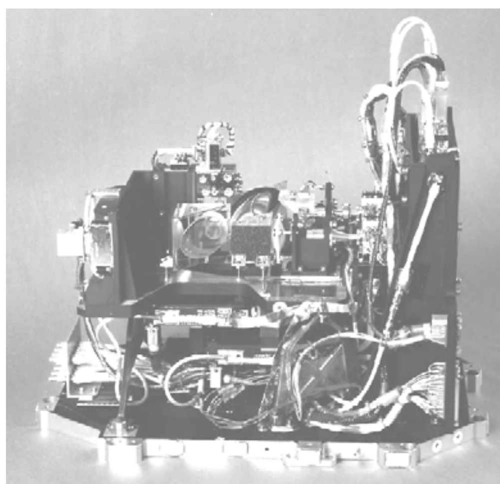

Fig. 1. Microwave Humidity Sounder, copyright 2003 EUMETSAT.

Table I shows the performance information for the MHS instrument. The radiometer performance is primarily driven by the radiometric sensitivity which expresses the capability to separate scene (or antenna) temperatures.

channel	H1	H2	H3	H4	H5
f_o	89	157	183.3	183.3	190.3
IF (GHz)	0.1 - 1.25	0.1 - 1.25	0.75 - 1.25	2.5 - 3.5	0.1 - 1.1
Temperature sensitivity (K)	0.22	0.52	0.24	0.21	0.57
Specified DSB equivalent temperature (K)	<920	<1540	<1582	<1763	<1763

TABLE I
THE PERFORMANCE INFORMATION FOR THE MHS INSTRUMENT

It is related to the noise nature of the useful signal after square-law detection:

$$\Delta T = T_{sys}\sqrt{\frac{1}{B\tau}+\left(\frac{\Delta G}{G}\right)^2} \quad (1)$$

where: T_{sys} is the System noise temperature, B is the RF pre-detection bandwidth, τ is the video integration time and $\frac{\Delta G}{G}$ is the short term overall gain stability.

In the Front Ends design two key performances are therefore to be optimised:

- The noise performance
- The gain stability performance.

Actually, most of the G-band (140 -220 GHz) receivers are realized using hybrid circuits including Schottky diodes. Fig. 2 represents the state-of-the-art of the noise performance of diodes and SIS based receivers in the G-band. As shown in Fig. 2, the noise performance of the receivers using HEMT LNAs are comparable with uncooled sub-harmonic pumping (SHP) Schottky receivers. Why cannot HEMT-based-receivers get higher performance? We are trying to answer by presenting in a first part the different HEMT technologies and their associated performance. The main intrinsic and parasitic parameters of short gate length HEMTs are analyzed in the second part.

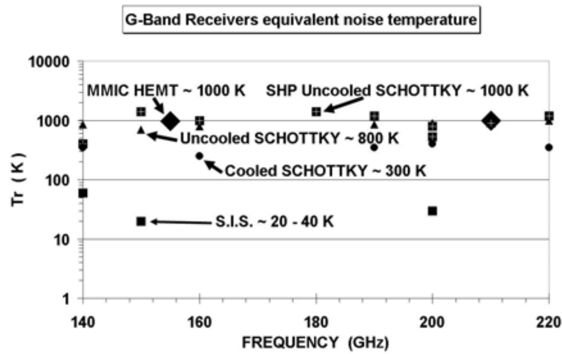

Fig. 2. Noise performance of G-band receivers.

II. HEMT STRUCTURES AND THEIR ASSOCIATED PERFORMANCE FOR MILLIMETER WAVE APPLICATIONS

A. HEMTs structures

The indium phosphide (InP)-based HEMTs has demonstrated its high-speed potentialities for mm-wave applications.

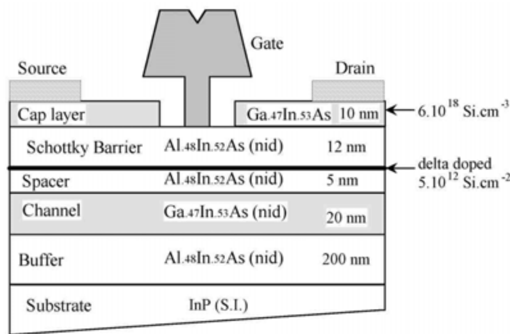

Fig. 3. Standard layer structure of lattice-matched HEMT on InP.

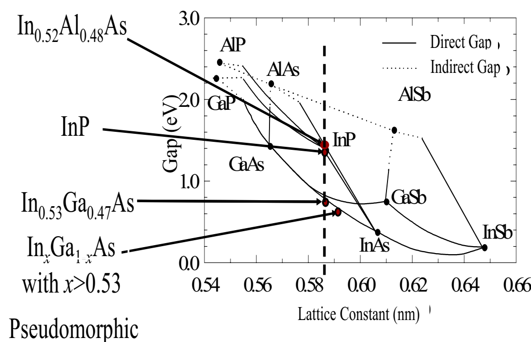

Fig. 4. Energy band gap versus lattice parameter of $In_xGa_{1-x}As$ and $In_yAl_{1-y}As$ materials for different Indium contents.

A standard layer structure (Fig. 3) is composed of a semi-insulating InP substrate followed by an InAlAs buffer layer, an InGaAs channel layer, an AlInAs spacer, a pulsed-doped donor layer, a Schottky barrier layer and finally an InGaAs cap layer. Using these indium compositions, both layers have same lattice parameter than the InP substrate (Fig. 4). Value of conduction band discontinuity ΔEc is close to 0.5 eV and leads a 2DEG carrier density higher than 3.10^{12} cm^{-2}. One way to improve the performance of HEMT on InP substrate consists to increase the Indium content in the channel that leads better transport properties.

On an other hand, metamorphic HEMTs (MM-HEMTs) using an $In_xAl_{1-x}As/In_xGa_{1-x}As$ heterostructure grown on GaAs substrate constitute a good alternative to lattice-matched HEMTs. Compared to using InP substrates, the MHEMT technology is less expensive, taking advantage of the rapidlygrowing size of GaAs wafers, up to 6 inch today. Using the metamorphic concept, the indium content of unstrained heterostructure can be chosen in the range 0.33 – 0.6 and more for pseudomorphic heterostructure; recent results [2] (NF=2.1 dB, G=13 dB at 94 GHz) of high performance W-band LNAs have been obtained with an indium content of 80%.

B. InP-based HEMTs performance

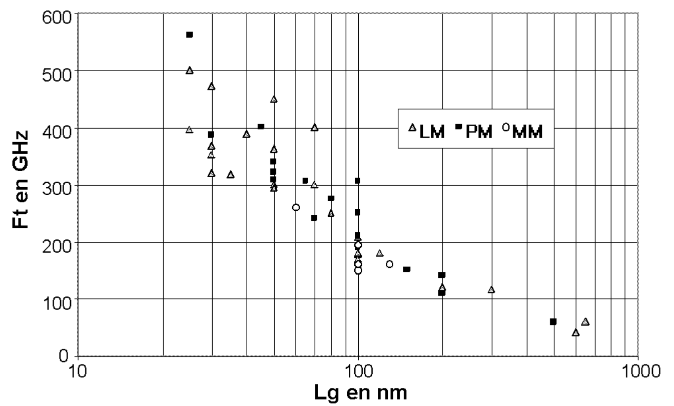

(a)

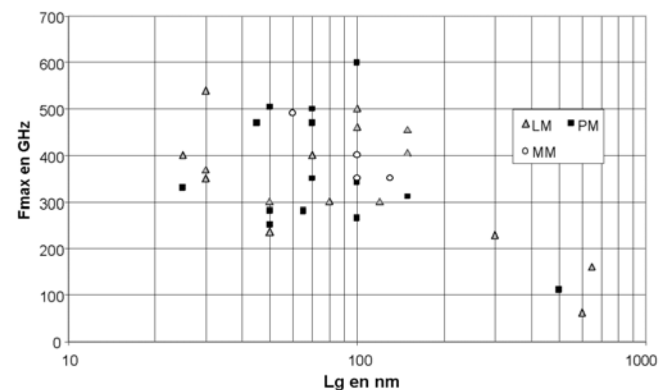

(b)

Fig. 5. State-of-the-art of InP-based HEMTs transit frequencies versus the gate length (a) f_t, (b) f_{max}.

Figure 5a shows the state of the art f_t values of InP-based HEMTs versus the gate length while Fig. 5b represents the values of f_{max}. f_{max} and f_t are defined respectively as the transit frequency (i.e. the gain is equal to 0 dB) for Mason's gain (*U*) and for the Current Gain ($|H_{21}|^2$). f_t continues to increase with the downscaling process and values higher as 562 GHz is obtained in the case of the

70% indium content pseudomorphic heterostructure with a gate length of 25nm [3]. f_{max} is also a very important criterion for low noise amplifiers and values close to 600 GHz is also obtained by the shortest gate length InP-based HEMTs. Contrary of f_t, f_{max} presents a saturation effect versus the downscaling process (for L_g<100 nm); the origins of this limitation will be discussed in the next paragraph. Fig. 6 represents the noise performance (G_{ass} versus NF_{min}) at 60 and 94 GHz of InP-based HEMTs. A value of 1.3 dB of NFmin with and associated available gain of 8.2 dB at 94 GHz has been reported in [4] for a 100nm gate length pseudomorphic InP-based HEMT. No results of NF_{min} in the G-band are reported in literature, simple extrapolation of these 94 GHz results should lead NF_{min} close to 3 dB at 200 GHz that is very optimistic as compared to G-band LNA's results (NF=5 dB at 155 GHz).

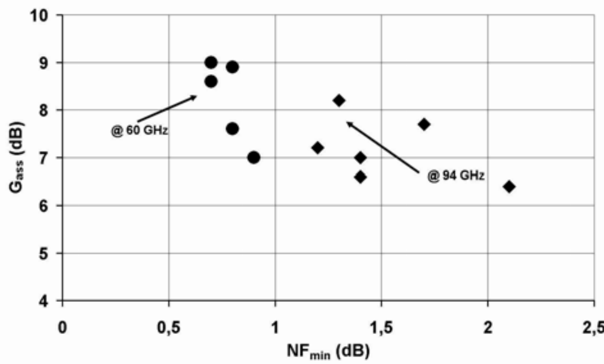

Fig. 6. State-of-the-art of the noise performance of InP-based HEMTs.

III. LIMITING PARAMETERS OF SHORT GATE LENGTH

f_{max} is one of the best criterion to compare the mm-wave performance of transistors, for both power and low noise applications. As shown in the approximated expression (2), f_{max} depends on both extrinsic (access resistances, parasitic capacitances) and intrinsic parameters (gate transconductance, output conductance, intrinsic capacitances). We can also approximate the minimum noise figure as function of f_{max} (equation 3); this approximated expression of NF_{min} is enough accurate even in the mm-wave because f_{max} includes all the intrinsic and extrinsic contributions.

$$f_{\max} \approx \frac{f_c}{2\sqrt{\left(R_g + R_s + R_i\right) \left(g_d + g_m \frac{C_{Miller}}{C_{gin}}\right)}} \quad (2)$$

$$NF_{\min} \approx 1 + \frac{f}{f_{\max}} \sqrt{P + R - 2C\sqrt{RP}} \sqrt{1 + (2\frac{f_{\max}}{f_c})^2 g_m (R_g + R_s + R_i)} \quad (3)$$

where P, R and C are dimensionless Pucel's noise parameters.

The improvements of f_{max}, by optimizing the HEMT structure and its associated technological processes, are very difficult and depend of several technological trade-offs. For the shortest gate length devices, the optimization window of f_{max} is very narrow that allows a slowing down of the increase of f_{max} versus the downscaling process (see Fig. 5b). Nevertheless, by considering the equation 2, it is possible to study the main dependences of f_{max} which we can classify into three groups:

- The intrinsic elements g_m, g_d, R_i and $f_c=g_m/2\pi C_{gs}$.
- The extrinsic element R_g, R_s.
- The mixed intrinsic/extrinsic elements C_{gin}, C_{Miller}.

This classification is not completely impartial and depends of the definition of the equivalent circuit and its extraction's accuracy.

The first important term of equation (2) is the intrinsic cutoff frequency, $f_c=g_m/2\pi C_{gs}$; this intrinsic cut-off frequency value keeps on following the conventional downscaling law. Consequently, this term is not a main limiting factor for f_{max}. A second term of equation (2) is the strong contribution of the access resistances R_g (gate resistance) and R_s (source resistance). These access resistances depend directly on the transistor topology; R_g is linear as function of the total gate width while R_s is inversely proportional. R_g depends also on the number of gate fingers (n_f) connected in parallel and varies proportionally to $1/(n_f)^2$. Moreover R_g and R_s depend of the downscaling process. Indeed R_g depends of several gate parameters (length, height, Mushroom width and shape, characteristic of the metal, width of the gate finger…). R_s depends also of a lot of technological parameters (gate to source distance, thickness and doping of the cap layer, alloyed or non-alloyed ohmic contacts, sheet resistance of the Schottky layer…). If we focus on the dependence of R_g and R_s versus the total gate width only, the minimum value of the sum $R_g + R_s$ (equation 2) is obtained for an optimal total gate width W_{topt} .

$$W_{topt} \approx \sqrt{\frac{3R_{so}}{R_m}} \quad n_f \quad (4)$$

where R_{so} is normalized source resistance (Ω.mm), R_m the normalized metallic gate resistance (Ω/mm) and n_f the number of gate fingers.

An other main limiting parameter of the increase of f_{max} is the ratio C_{gin} / C_{Miller} (see equation 2) where $C_{gin} \sim C_{gs} + C_p + C_{po}$ and $C_{Miller} \sim C_{gd} + C_p + C_{po}$ (symmetric source-gate-drain structure).

C_{gs} and C_{gd} are the intrinsic charge control capacitances, $C_p + C_{po}$ is a parasitic capacitance distributed along the source and gate metallization (see figure 7); C_p is assumed to be dependent with the finger width while C_{po} (1-2 fF typical) is assumed to be independent. These parasitic capacitances are almost in parallel with the intrinsic capacitances C_{gs} and C_{gd} and directly contribute to the degradation of the mm-wave performance.

® SILVACO simulations show that these parasitic capacitances are mainly located between the cap layer region (if not depleted) and the bottom of the mushroom. Then the value of C_p is strongly dependent of the gate foot height, the doping and thickness of the cap layer. For

a 6 10^{18} cm^{-2} doping cap layer with a thickness of 10 nm, this region is depleted due to the surface potential and the calculated value (® SILVACO) of C_p is close to 40 fF/mm. With a silicon nitride passivation, C_p increases to 170 fF/mm.

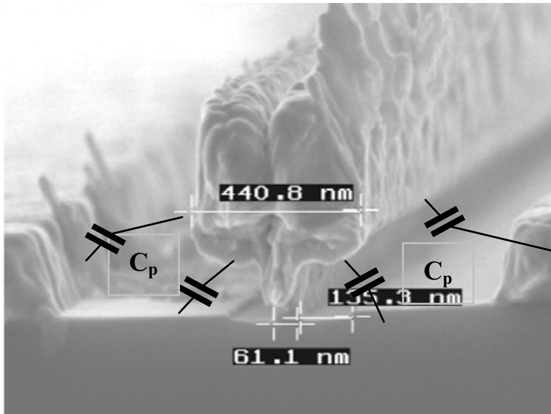

Fig. 7. Photography (MEB) of the cross section of a 60 nm gate length LM-HEMT.

Using a simple calculation, Fig. 8 shows the variation of $R_g + R_s$ and the C_{gin} / C_{Miller} versus the total gate width for a two fingers 70nm gate length LM-HEMT ($R_m = 480$ Ω/mm, $R_{so} = 0.35$ $\Omega.mm$, $C_{gs} = 720$ fF/mm, $C_{gd} = 90$ fF/mm, $C_{p_air} = 40$ fF/mm and $C_{p_Si3N4} = 170$ fF/mm, $C_{po} = 1fF$). The minimum value of W_t is strongly related both to the increase of $R_g + R_s$ and the decrease of the capacitance ratio. The maximum value of W_t is chosen to minimize the effect of the output conductance g_d (proportional to the gate width). For mm-wave applications with such device, the minimum value of the total gate width W_t is close to 70 µm while its maximum value is about of 100 µm for a two fingers HEMT.

Otherwise some intrinsic parameters in equation 2 contribute to decrease f_{max}. The intrinsic resistance R_i, associated with C_{gs} in a conventional equivalent circuit, also should be influent on the decrease of f_{max}. Physical based simulations and experimental results demonstrated that this resistance is inversely proportional to the intrinsic transconductance. Consequently, this intrinsic resistance cannot be, from theoretical point of view, a limitation to the increase of f_{max} along with the downscaling process of channel gate length. Finally, the increase of the output conductance g_d with the reduction of gate channel length is one of the well known short channel effect of FET devices. The origin of the increase of g_d is due to numerous parameters. Many solutions to improve the efficiency of the channel control by the gate have been proposed. One of them [5] consists to optimize the epitaxial structure along the downscaling of the gate by reducing the thickness of Schottky, spacer and active layers to increase the aspect ratio. The window of such optimization for sub-70nm node is very narrow. Indeed the decrease of the EPI layers induces several parasitic effects (Tunnel conduction, modulation of the channel by the surface charges, direct injection into the buffer…).

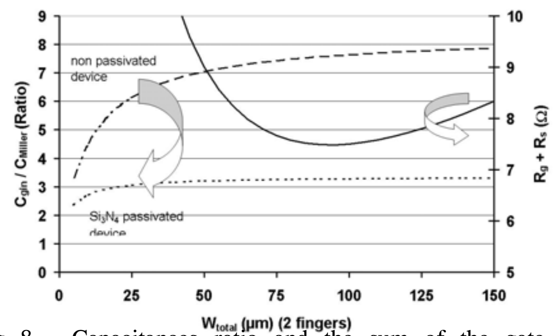

Fig. 8. Capacitances ratio and the sum of the gate and source resistances versus the total gate width for a 70nm InP-based HEMT.

VI. CONCLUSION

The key performance of a G-band receiver for atmospheric sounder applications is the low noise and high gain stability. Short gate length InP-based HEMTs are a good alternative to conventional Schottky-diodes-based down converters. Nevertheless the performance (f_{max}, $gain$, T_{min}) of InP-based HEMTs tend to saturate with the downscaling process. f_{max} is one of the best criteria to compare the microwave performance of transistors, for analog applications. The first limiting parameter of f_{max} is the access resistances, the second limiting parameter is the C_{gin}/C_{Miller} ratio and the third ones is the intrinsic output conductance g_d Solutions of optimization to improve the performance of both active and passive devices in G-band for the realization of MMIC will be presented.

This work is performed under ESA contract – TENDER AO/1-4060/01/NL/DC- "MMIC Technology for Future Atmospheric Sounders".

REFERENCES

[1] Arlindo Arriaga, « Microwave Humidity Sounder (MHS) Simulations with a radiative transfer model", Technical Department Technical Memorandum No. 5, March, 2000.

[2] A. Tessmann, A. Leuther, C. Schwoerer, H. Massler, S. Kudszus, W. Reinert, M. Schlechtweg, « A coplanar 94 GHz low-noise amplifier mmic using 0.07 µm metamorphic cascode hemts. », Proc. of IMS2003,pp. 1581-1584.

[3] Y. Yamashita, A. Endoh, K. Shinohara, K. Hikosaka, T. Matsui, S. Hiyamizu, T. Mimura, "Pseudomorphic $In_{0.52}Al_{0.48}As/In_{0.7}Ga_{0.3}As$ HEMTs With an Ultrahigh f_T of 562 GHz", IEEE Electron Device Letters, vol. 23, no. 10, pp. 573-575, October 2002.

[4] K. L. Tan, D. C. Streit, P. D. Chow, R. M. Dia, A. C. Han, P.H. Liu, D. Garske, R. Lai, "140 GHz 0.1 µm gate-length pseudomorphic In0.52Al0.48As/In0.60Ga0.40As/InP HEMT", Proc. ofIEDM 1991, pp. 239-242.

[5] T. Parenty, S. Bollaert, J. Mateos, X. Wallart, A. Cappy, "Design and realization of sub 100nm gate length HEMTs" IPRM 2001, pp. 624-627.